



Research paper

Special features of double pulsed gas metal arc welding

L.L. Wang^{a,b}, H.L. Wei^b, J.X. Xue^a, T. DebRoy^{b,*}^a School of Mechanical and Automotive Engineering, South China University of Technology, Guangzhou 510641, China^b Department of Materials Science and Engineering, The Pennsylvania State University, University Park, PA 16802, USA

ARTICLE INFO

Keywords:

Double pulsed welding
 Numerical simulation
 Current amplitude
 Cooling rate
 Grain refinement

ABSTRACT

Since the pulsation of heat input provides a flexible and effective way to control temporal variation of weld pool geometry, cooling rate and solidification parameters, double pulsed (DP) gas metal arc welding (GMAW) serves as a unique tool for controlling the structure and properties of welds. A comprehensive model of DP-GMAW, when adequately tested with experimental data, provides a powerful tool for achieving predictable, high-quality welds. Here we develop a three-dimensional, transient, numerical model of DP-GMAW and test it against carefully planned experiments. The variation of current amplitude enables tailoring of weld attributes such as geometry, cooling rates, solidification parameters and microstructure and its role in the welding of an aluminum alloy is examined both experimentally and theoretically. Since the grain size in the fusion zone is significantly affected by its cooling rate, experimental measurements of grain size for various current amplitudes are correlated with the corresponding computed cooling rates at a constant heat input. Results indicate that cooling rates can be increased and grain size can be refined at a constant heat input while using DP-GMAW. The current amplitude of DP-GMAW can be used to adjust the average cooling rate without changing the heat input. The effects of current amplitude on the fusion zone geometry, cooling rates, solidification parameters, and grain size are investigated for improved understanding of DP-GMAW.

1. Introduction

Gas metal arc welding (GMAW) is the most widely used welding process because of its ability to bridge gaps in large butt joints and tailor weld metal composition and properties by appropriate selection of filler metal at low cost. An important variable in GMAW is the heat input that represents the amount of energy deposited per unit length. Reduction of heat input results in smaller molten pool, narrower size of the heat affected zone and improved weld quality. In GMAW, lower heat input is often achieved by current pulsing to reduce the average current. In automotive and sheet metal industries where welding of thin sheets is important, pulsed current GMAW, otherwise known as single pulsed (SP) GMAW provide superior control of metal droplet transfer from the melting filler wire to the liquid weld pool. The droplet transfer mode achieved in SP-GMAW is spray transfer with one molten metal drop transferred from the melting electrode into the weld pool in each current pulse. This mode of metal transfer provides excellent surface finish and significantly reduced spatter. Since a high pulsing frequency of up to several hundred pulses per second is used, the pool shape and size and the cooling rate of the fusion zone does not change with time after the initial start of welding. The fusion zone size and cooling rate depend on the welding current and the heat input. In other words, in

SP-GMAW, control of cooling rate, which influences the microstructure and properties of welds is achieved by selecting the heat input, just like the practice in other fusion welding processes.

A variant of pulsed GMAW, known as double pulsed (DP) GMAW has changed the interrelation between cooling rate and heat input, because it enables adjustment of various weld attributes at a constant heat input by changing the pulsing parameters. Fig. 1 illustrates schematically the typical current waveform of DP-GMAW. As shown in the figure, pulsing in DP-GMAW involves repeated application of two sequential phases of somewhat different pulsing characteristics. Both the first and second phases contain several current pulses at high frequencies, and Liu et al. (2013a) have discussed that these current pulses are used to achieve the metal transfer in spray transfer mode. However, the base current and number of current pulses during the first phase are higher than those during the second phase. Consequently, the average current of the first phase (I_F) is higher than that in the second phase (I_S). An important variable in DP-GMAW is the current amplitude (A) which is defined as half of the difference between I_F and I_S . DP-GMAW has been used for the welding of aluminum alloys because of its ability to provide reduced porosity in the weld metal as reported by Mathivanan et al. (2014), better gap bridging ability as demonstrated by Yamamoto et al. (1992), and better ability to control the mode of droplet transfer,

* Corresponding author.

E-mail address: rtd1@psu.edu (T. DebRoy).<http://dx.doi.org/10.1016/j.jmatprotec.2017.08.039>

Received 5 July 2017; Received in revised form 23 August 2017; Accepted 26 August 2017

Available online 30 August 2017

0924-0136/ © 2017 Elsevier B.V. All rights reserved.

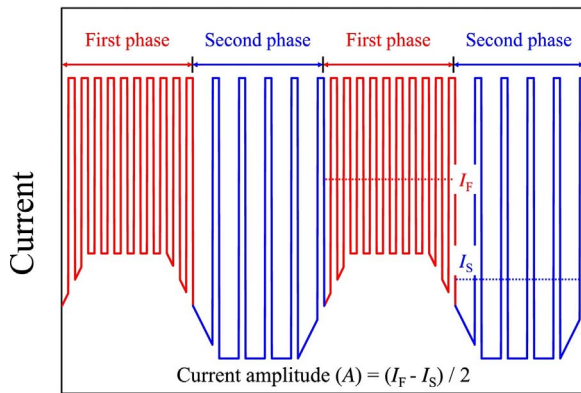


Fig. 1. Schematic diagram of current waveform of DP-GMAW. Current amplitude (A) is defined as half of the difference between the average current of the first phase (I_F) and the average current of the second phase (I_S).

all of which affect weld quality.

Sen et al. (2015) established that heat input was time-dependent and related to the temporal variation of arc current during DP-GMAW. Liu et al., (2013b) observed that the geometry of the weld pool varied with time in DP-GMAW due to the variation of current waveform and heat input. Wang et al., (2016b) found that DP-GMAW typically produced a wavy weld penetration and the temporal variation of weld pool depth depended on pulsing parameters. Other weld attributes such as the cooling rate and solidification parameters also vary with time. Yamamoto et al. (1993) found that mean grain size could be reduced by using of DP-GMAW. Wang et al., (2017b) observed that double pulsed gas tungsten arc welding (GTAW) produced finer dendrite than that produced by conventional pulsed GTAW. Wang et al., (2016a) are ported that the scale of the dendrite could be changed through changing the current period of DP-GMAW while keeping the mean welding current and heat input constant.

Although the advantages of DP-GMAW has been well documented in the literature, the mechanisms for these observations are not well understood. Here we develop a phenomenological model based on the scientific principles to better understand the origins of the improvements achievable by DP-GMAW. The equations of conservation of mass, momentum, and energy are solved with appropriate boundary conditions to examine the role of important variables in DP-GMAW for various welding conditions. Periodic variations of fusion zone geometry, liquid metal flow fields, temperature distributions, cooling rates and solidification parameters are examined. Experiments are conducted to verify the calculations. Remelting and resolidification of the previously solidified metal near the trailing edge of the weld pool are studied. Grain refinement of 1060 aluminum welds is characterized experimentally, and its mechanism is examined by using the estimated mean cooling rate.

2. Materials and methods

2.1. Materials and process parameters

Aluminum alloy AA1060 was welded using ER1070 filler metal. Table 1 shows the chemical compositions of the base metal and the

Table 1
Chemical compositions of AA1060 and ER1070 (wt%).

Material	Fe	Si	Cu	V	Zn	Mg	Mn	Ti	Al
AA1060 (base metal)	0.35	0.25	0.05	0.05	0.05	0.03	0.03	0.03	Balance
ER1070 (filler wire)	0.25	0.20	0.04	0.05	0.04	0.03	0.03	0.03	Balance

Table 2
Welding process parameters.

Process parameters	No. 1	No. 2	No. 3	No. 4
Mode of welding current	SP-GMAW	DP-GMAW	DP-GMAW	DP-GMAW
Current amplitude (A)	0	30	40	50
Mean voltage (V)	22.3	22.3	22.3	22.3
Mean current (A)	100	100	100	100
Welding speed (mm s^{-1})	8	8	8	8
Current period (s)	–	0.4	0.4	0.4
First phase mean current (A)	–	130	140	150
Second phase mean current (A)	–	70	60	50
First phase time (s)	–	0.2	0.2	0.2
Second phase time (s)	–	0.2	0.2	0.2

filler wire given by Liu et al., (2013c). The base metal plates were 200 mm long, 80 mm wide and 4 mm in thickness and the filler wires had a diameter of 1.2 mm. Bead-on-plate welding was carried out using a digital welding power source. The shielding gas was 99.99% argon with gas flow rate of 15 l/min, and the electrode extension was 15 mm. Specimens were cut along the central longitudinal and transverse sections of welds after welding. The samples were ground and polished to 0.06 μm using colloidal silica and subsequently were electrolytically etched using the standard Barker's reagent (2.5 ml HBF_4 + 100 ml H_2O) with 120 s. The metallographic images were taken using a polarized microscope.

The welding process parameters are presented in Table 2. Cases 1 and 3 are used to compare SP-GMAW and DP-GMAW. Cases 2, 3 and 4 are used to study the effect of current amplitude on fusion zone sizes and solidification parameters of DP-GMAW. The actual welding current waveforms of cases 2, 3 and 4 are shown in Fig. 2. As shown in the figure, greater current amplitude results in an increase in the average current of the first phase (I_F) and decrease in the average current of the second phase (I_S). Note that all the cases have the same heat input and welding speed.

2.2. Numerical methods

2.2.1. Heat transfer and fluid flow model

The heat transfer and fluid flow in the weld pool are calculated by solving the equations of conservation of mass, momentum, and energy in three dimensions as summarized by Wei et al. (2015) and Wei et al., (2017). The model considers the effect of Marangoni stress, electromagnetic force and buoyancy on liquid metal convection within the weld pool, as discussed by David and DebRoy (1992). The governing equations and boundary conditions have been shown by Wei et al. (2016) and Mishra et al. (2008), and they are not repeated here. The liquid metal droplets from the tip of the filler wire were transported into the melt pool with one droplet per current pulse. Kim et al. (2003) proposed a volumetric heat source to account for the energy transferred by the overheated droplets, and the volumetric heat source was incorporated in the model. The thermophysical properties used in the calculation of temperature and velocity fields are presented in Table 3.

The pulsing current of SP-GMAW in the model is implemented as constant mean current of 100 A. Such a simplification offers enhanced computational efficiency without affecting the accuracy of the calculations. The current pulsing frequency of SP-GMAW was 80 Hz, Wang et al. (2014) experimentally and Liu et al. (2015) numerically found that the weld penetration depth remained constant with time due to short application times for the high and low current pulses under such high frequency. The mean currents during the first and the second pulse phases of the DP-GMAW are implemented in a similar way to that of the SP-GMAW. Roy et al. (2006) proposed a method for unsteady-state welding, the model stored spatial distribution of temperature and velocity at the ending time of the first phase, which were loaded at the starting time of the second phase, and vice versa. The temperature field,

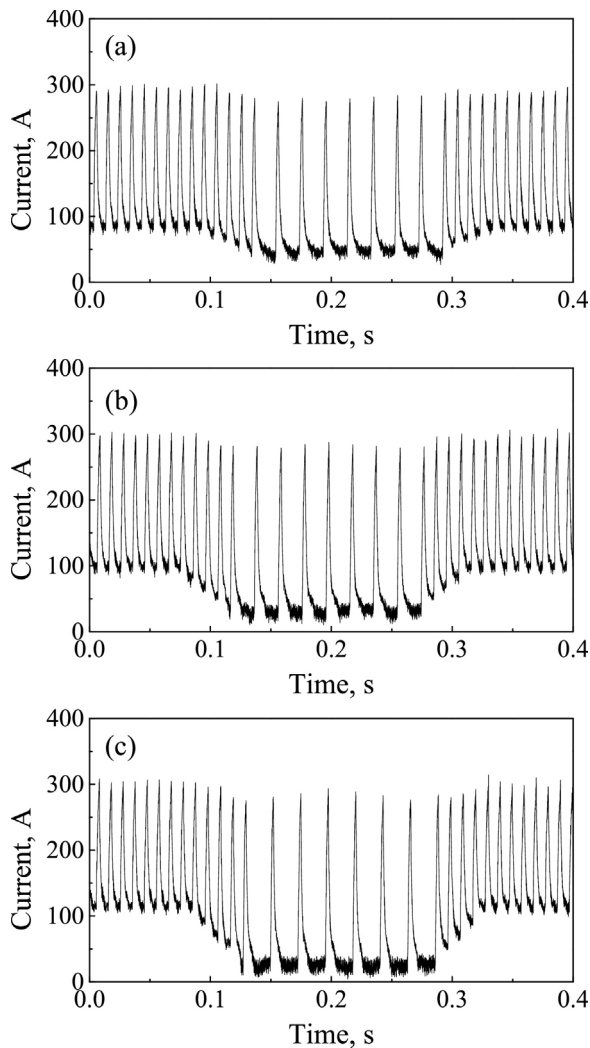


Fig. 2. Welding current waveform of DP-GMAW with different current amplitude. (a) 30 A; (b) 40 A; (c) 50 A.

Table 3

Data used for the calculations of weld pool temperature and velocity fields.

Variables and unit	Value
Density of liquid metal (kg m^{-3})	2400
Viscosity of liquid ($\text{kg m}^{-1} \text{s}^{-1}$)	0.001
Solidus temperature (K)	919
Liquidus temperature (K)	930
Enthalpy of solid at melting point (J kg^{-1})	6.25×10^5
Enthalpy of liquid at melting point (J kg^{-1})	9.98×10^5
Specific heat of solid ($\text{J kg}^{-1} \text{K}^{-1}$)	900
Specific heat of liquid ($\text{J kg}^{-1} \text{K}^{-1}$)	1170
Thermal conductivity of solid ($\text{W m}^{-1} \text{K}^{-1}$)	168
Thermal conductivity of liquid ($\text{W m}^{-1} \text{K}^{-1}$)	108
Coefficient of thermal expansion (K^{-1})	2.375×10^{-5}
Temperature coefficient of surface tension ($\text{N m}^{-1} \text{K}^{-1}$)	-3.5×10^{-4}

liquid metal flow field, and thermal history are calculated from the model.

2.2.2. Calculation of solidification parameters

The temperature gradient (G), growth rate (R) and their combined form GR which represents cooling rate are important solidification parameters. Their values are temporally and spatially variable, which are calculated from the temperature field. The value R was calculated at the trailing edge of the melt pool on the top surface using the following

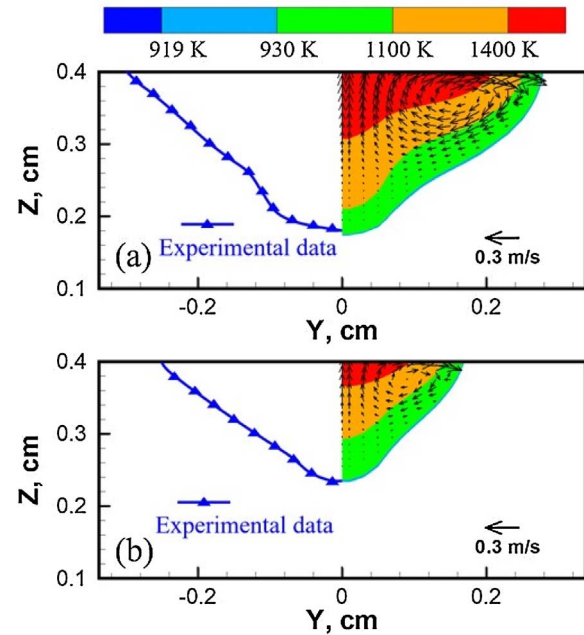


Fig. 3. Comparison of the calculated and experimental weld profiles of DP-GMAW in the transverse section. (a) Largest weld profile produced at 0.2 s; (b) Smallest weld profile produced at 0.4 s. Detailed process parameters are from case 3 of Table 2. The experimental data depicting the boundary of the fusion zone are shown in blue triangles on the left-hand side. The computed weld profiles are shown in the right-hand side. (For interpretation of the references to colour in this figure legend, the reader is referred to the web version of this article.)

relation:

$$R = \frac{\Delta d_s}{\Delta t} \quad (1)$$

where Δd_s is the displacement of the trailing edge during a short time interval of Δt . The cooling rate was calculated at the trailing edge of the melt pool on the top surface for microstructure evaluation.

3. Results and discussions

3.1. Weld dimensions

In order to validate the heat transfer and fluid flow model, the calculated and experimentally observed results of DP-GMAW are compared. Fig. 3 shows the maximum and minimum transverse cross-sections of the fusion zone produced by DP-GMAW in a single period. The process parameters used for the experiments are presented in Table 2 as case 3. The transverse cross sections were obtained in two steps. First, the sample was sectioned along the central longitudinal plane to determine the maximum and minimum penetrations. Subsequently, the sample was cut in transverse sections to obtain the maximum and minimum weld cross-sections. Fig. 3 shows that the calculated weld dimensions agree fairly well with the corresponding experimental results. The agreement indicates the validity of the modeling results, which are further used to compute the solidification parameters.

The heat input changes periodically during DP-GMAW due to current pulsing. Fig. 4 shows the calculated temporal variation of weld dimensions of SP-GMAW and DP-GMAW with different current amplitudes (30 A, 40 A, and 50 A). The weld width and weld penetration of DP-GMAW welds vary with time in a periodic manner, which is consistent with the temporal variation of heat input. For DP-GMAW, the width and penetration of the weld increase with time during the first phase (0 s–0.2 s) due to high heat input. Maximum width and penetration of weld are produced at the end of the first phase. Both width and penetration of weld experience a faster increase with greater

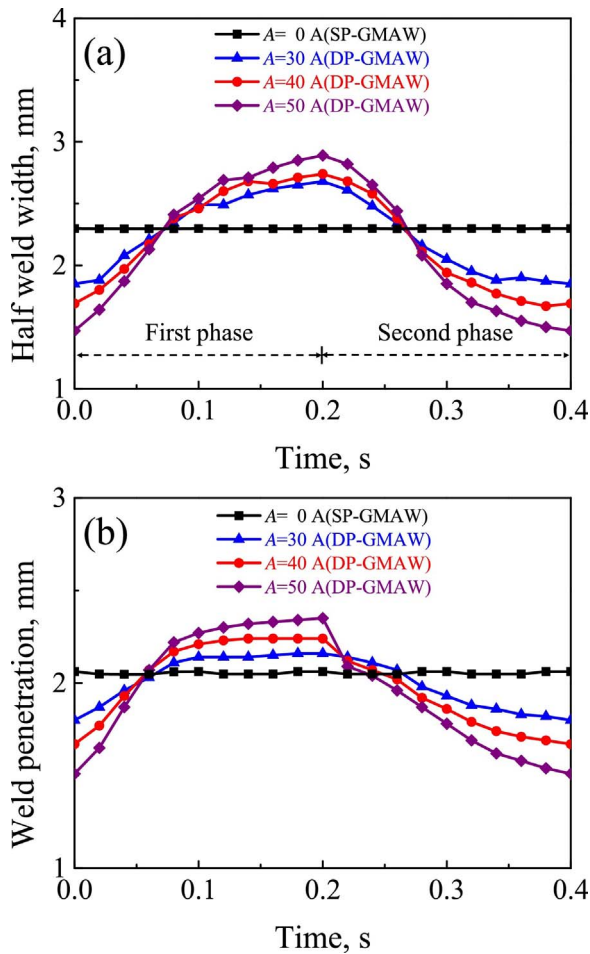


Fig. 4. Calculated temporal variation of weld profile dimensions of SP-GMAW and DP-GMAW with different current amplitudes (A). (a) Half weld width; (b) Weld penetration.

current amplitude, maximum width and penetration of weld increase with higher current amplitude. The width and penetration of weld decrease with time during the second phase (0.2 s–0.4 s) due to low heat input. Minimum width and penetration of weld are produced at the end of the second phase as anticipated. Both width and penetration of weld experience a faster decrease with greater current amplitude, minimum width and penetration of weld decrease with greater current amplitude. Therefore, current amplitude should be limited to an appropriate value to ensure effective weld penetration. Greater current amplitude means the larger difference in the heat input of the first and second phases for DP-GMAW. The greater current amplitude enhances the periodic expansion and contraction of the weld pool. The maximum weld penetration increases and minimum weld penetration decreases with greater current amplitude.

Fig. 5 shows the calculated temperature and velocity profiles of DP-GMAW during a current period of 0.4 s. The process parameters are presented in Table 2 as case 3. On the top surface of the weld pool, the liquid metal flows from the center to the edge mainly driven by Marangoni stress. Wei et al., (2017) indicated that the Marangoni stress was from the spatial gradient of surface tension. The liquid metal circulates with the maximum velocity of about 0.8 m/s in the weld pool. Peclet number (Pe) is the ratio of rate of heat transfer by convection and conduction, i.e., the mechanism of heat transfer within the weld pool:

$$Pe = \frac{\mu \rho C_p L_R}{k} \quad (2)$$

where μ is the velocity of the liquid metal (cm/s), ρ is the density of the liquid metal (g/cm^3), C_p is the specific heat (cal/g K), L_R is the

characteristic length (cm), k is the thermal conductivity (cal/cm s K). Here, the value of Pe is about 51 which indicates that heat is transported within the melt pool mainly by convection. Fig. 5(a)–(c) show that the weld pool expands during the first phase (0 s–0.2 s) due to high heat input. Fig. 5(d) and (e) show that the weld pool shrinks during the second phase (0.2 s–0.4 s) due to low heat input.

The motion of the trailing edge of the weld pool deviates significantly from the welding speed due to time-dependent change of the weld pool size. Fig. 6 shows the comparison of the movement of the trailing point of DP-GMAW and SP-GMAW. The moving speed of the trailing edge during SP-GMAW is identical to the welding speed, which results in a linear correlation between the location and the time. However, it is nonlinear for DP-GMAW because of the time-dependent changes in the fusion zone dimensions. The trailing point moves slowly during the first phase while it moves significantly faster during the second phase. Note that the trailing point moves backward from 0.04 s to 0.1 s due to the considerable expansion rate of the weld pool compared with the welding speed.

Unusual remelting and re-solidification of the previously solidified metal occur due to the periodic expansion and contraction of the weld pool. Fig. 7 shows the variation of the weld pool boundary from 0 s to 0.1 s to further examine this phenomenon. It can be observed that the weld pool trailing edge moves opposite to the welding direction from 0.04 s to 0.1 s, although the heat source is moving along welding direction. Therefore, remelting of the previously solidified fusion metal occurs at the trailing edge of the weld pool. This remelting and re-solidification affects the solidification parameters as will be discussed later in this paper.

3.2. Solidification parameters

Fig. 8 shows the calculated temporal variation of solidification growth rate, R and the cooling rate, GR , at the weld pool trailing edge of SP-GMAW and DP-GMAW. Different from SP-GMAW, R and GR are time dependent for DP-GMAW. Wang et al., (2017a) revealed that the variations of R and GR resulted from the periodic expansion and contraction of the weld pool. For DP-GMAW, the weld pool expansion direction at the trailing edge is opposite to the welding direction during the first phase (0 s – 0.2 s). Therefore, the local solidification rate R is less than the welding speed by an amount equal to the melt pool expansion speed. R decreases rapidly to zero during the first phase, which means that the melt pool expansion speed at the trailing edge is equal to the welding speed. Then R keeps at zero during the time interval (Δt_r), which means that solidification stops and remelting occurs at the trailing edge of the weld pool. When the current amplitude increases from 30 A to 40 A and 50 A, Δt_r increases from 0.04 s to 0.08 s and 0.10 s during a current period which is 0.40 s. During the second phase (0.2 s–0.4 s), the moving direction of the melt pool trailing edge is identical to the welding direction, which results in higher R than the welding speed due to the contraction of the weld pool. R increases progressively between 0.2 s and 0.3 s due to increasing weld pool contraction speed, then decreases gradually between 0.3 s and 0.4 s due to decreasing weld pool contraction speed. In addition, R is greater during the entire second phase than that during the first phase.

Here, SP-GMAW is considered as a special case of DP-GMAW with zero current amplitude. With the current amplitude increasing from 0 A to 30 A, 40 A and 50 A, the actual solidification time of DP-GMAW during a current period decreases from 0.40 s to 0.36 s, 0.32 s and 0.30 s. The decrease of actual solidification time results in the increase in average R with greater current amplitude. With the current amplitude increasing from 0 A to 30 A, 40 A and 50 A, the average R increases from 8.0 mm/s to 9.0 mm/s, 10.6 mm/s and 11.9 mm/s. Due to the insignificant change of G , the average cooling rate increases from 3267.0 K/s to 3526.8 K/s, 4014.0 K/s and 4486.0 K/s, respectively, which is presented in Table 4. The calculated results indicate that: (i) cooling rate can be increased at constant heat input while using DP-

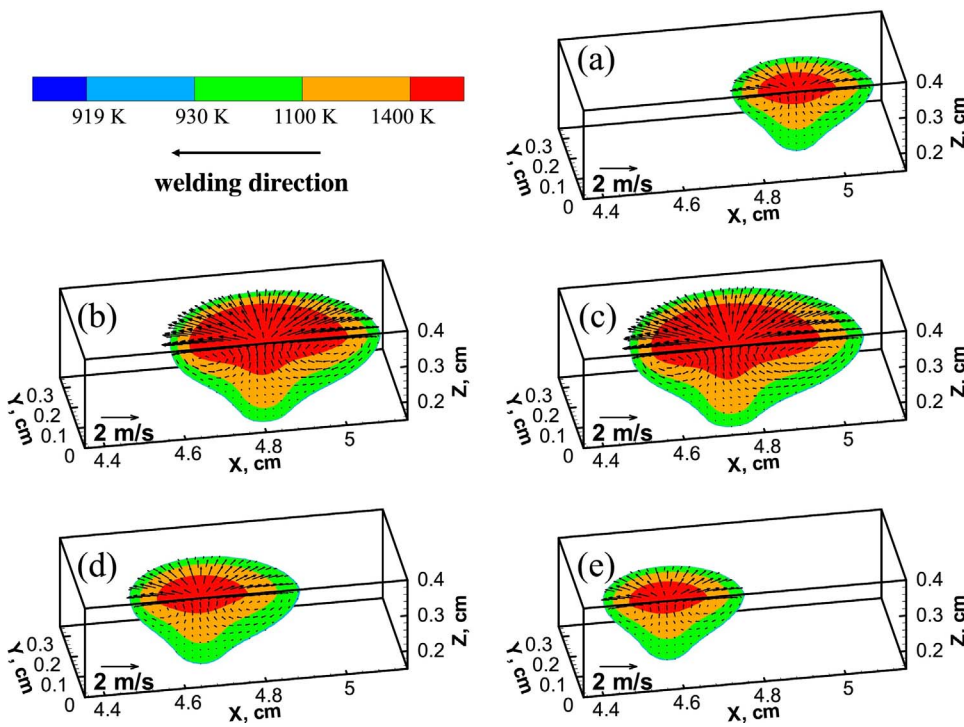


Fig. 5. Temperature and velocity fields of DP-GMAW during a current period. (a) 0.0 s; (b) 0.1 s; (c) 0.2 s; (d) 0.3 s; (e) 0.4 s. Detailed process parameters are from case 3 of Table 2.

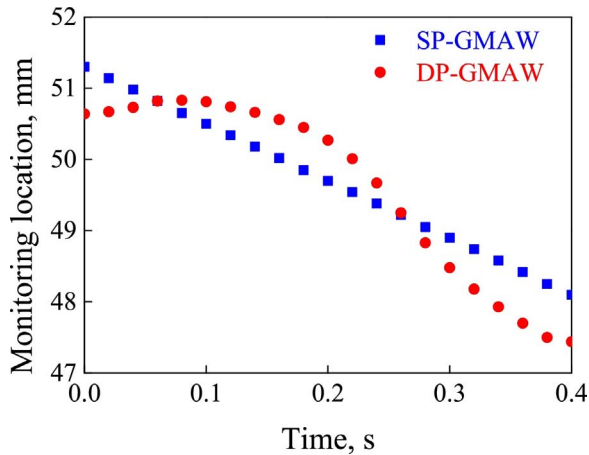


Fig. 6. Movement of the monitoring location of SP-GMAW and DP-GMAW during a current period.

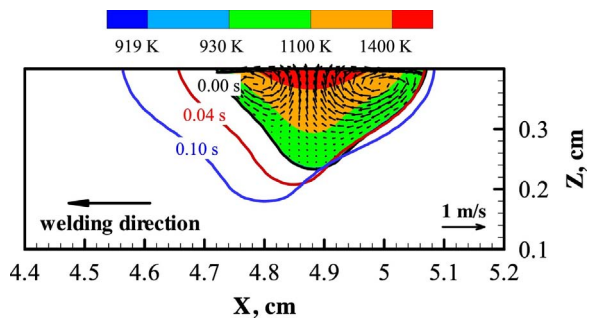


Fig. 7. Weld pool boundary of DP-GMAW in the longitudinal section from 0 to 0.1 s. Detailed process parameters are from case 3 of Table 2.

GMAW compared with SP-GMAW; (ii) cooling rate can be increased at constant heat input while increasing current amplitude during DP-GMAW. In addition, cooling rate during the second phase is evidently higher than that during the first phase.

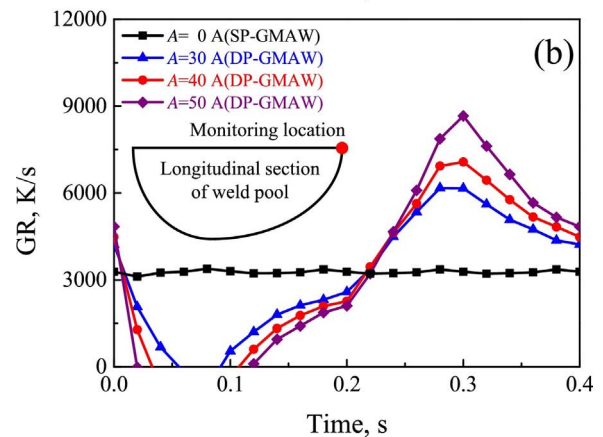
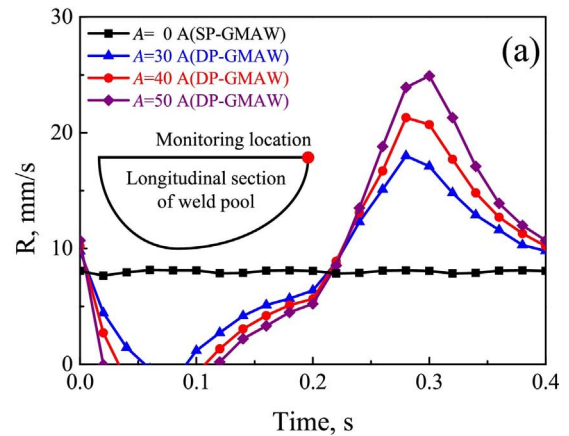


Fig. 8. Calculated temporal variation of solidification parameters at weld pool trailing edge of SP-GMAW and DP-GMAW. (a) R; (b) GR.

Fig. 9 shows the thermal cycles recorded at five monitoring points on the top surface of the weld along the centerline during SP-GMAW and DP-GMAW. X_0 is the first monitoring point. The distance between

Table 4
Calculated mean R and GR with different current amplitudes (A).

Process parameters	Mean R (mm/s)	Mean GR (K/s)
SP-GMAW (A = 0 A)	8.0	3267.0
DP-GMAW (A = 30 A)	9.0	3526.8
DP-GMAW (A = 40 A)	10.6	4014.0
DP-GMAW (A = 50 A)	11.9	4486.0

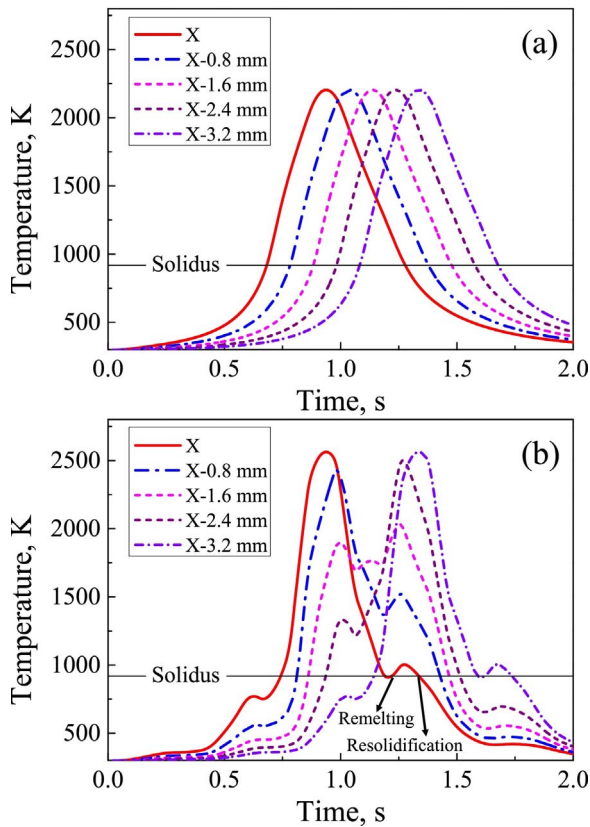


Fig. 9. Thermal cycles recorded by five monitoring points on the central top surface of the weld. (a) SP-GMAW; (b) DP-GMAW.

the first and the fifth monitoring points (3.2 mm) covers the displacement of the heat source in a time interval of 0.4 s with welding speed of 8 mm/s. No significant change in the temperature-time curve is observed among different monitoring locations for SP-GMAW, which is consistent with the cooling rate in Fig. 8(b). However, the temperature-time curve varies significantly for DP-GMAW. The variation results from the periodic changes of the heat input and weld pool shape during DP-GMAW. The inflections in the temperature-time curves of DP-GMAW are owing to the local heating and cooling due to the expansion and contraction of the weld pool. Remelting and re-solidification near the trailing edge of the weld pool during DP-GMAW phenomenon are observed. Another outcome is that the cooling rate of DP-GMAW is time-dependent, which is also consistent with the results presented in Fig. 8(b).

3.3. Grain structure refinement by changing current amplitude

Fig. 10 shows the macrostructure from the central longitudinal section of welds by SP-GMAW and DP-GMAW with different current amplitudes. The microstructures were obtained from the same location of the welds. The fusion line is marked by a white line in Fig. 10. For DP-GMAW, the difference between the minimum penetration and maximum penetration increases with greater current amplitude. The

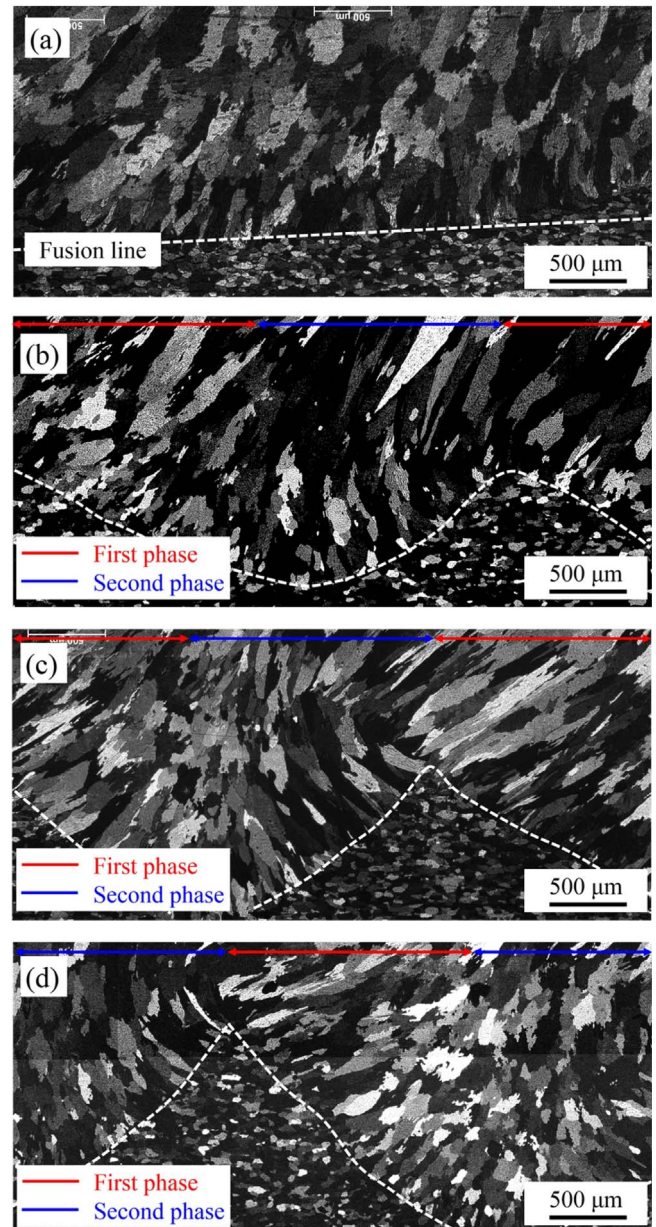


Fig. 10. Macrostructure from the central longitudinal section of the weld by SP-GMAW and DP-GMAW with different current amplitudes. (a) SP-GMAW; (b) DP-GMAW with current amplitude of 30 A; (c) DP-GMAW with current amplitude of 40 A; (d) DP-GMAW with current amplitude of 50 A.

experimental results coincide reasonably with the calculated weld profile dimension. Furthermore, the DP-GMAW welds are almost free from defects such as macroporosity, lack of fusion, and solidification cracking in the present area, which provide additional evidence that DP-GMAW is a feasible process for welding of aluminum. The length of displacement of heat source during a current period is 3.2 mm. While the length of each metallography is 4.2 mm, which is long enough for assessment of grain size. The different grains can be distinguished clearly by contrast, no equiaxed grains are observed in all the SP-GMAW and DP-GMAW welds. As reported by David and Vitek (1989), the cooling rate, GR, significantly affects the size of solidification structure. To examine that the scale of the solidification structure is affected by the cooling rate, the average grain size is computed along the vertical direction of welds by general intercept procedures based on ASTM E112.

Fig. 11 shows the measured grain size produced by different current amplitudes. Here, SP-GMAW is considered as a special case of DP-

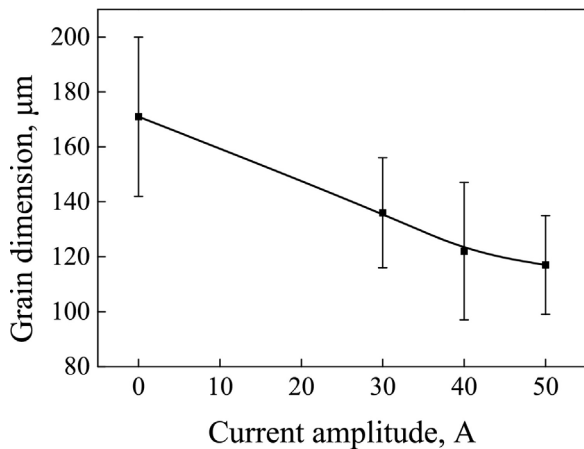


Fig. 11. Grain dimension produced by different current amplitudes of DP-GMAW at same heat input.

GMAW with zero current amplitude. With the current amplitude increasing from 0 A to 30 A, 40 A and 50 A, the grain size along the vertical direction of DP-GMA welds decreases from $171 \pm 29 \mu\text{m}$ to $136 \pm 20 \mu\text{m}$, $122 \pm 25 \mu\text{m}$ and $117 \pm 18 \mu\text{m}$, respectively. Although the mean welding current and heat input of SP-GMAW and DP-GMAW are the identical, experimental results indicate that: (i) grain size can be reduced at constant heat input while using DP-GMAW; (ii) grain size can be reduced at constant heat input while increasing current amplitude during DP-GMAW. In addition, grains produced during the second phase are evidently smaller than that generated during the first phase due to higher solidification growth rate and cooling rate. Both average grain size and distribution characteristic of grain size show good agreement with the calculated results.

4. Conclusions

Temporal variations of three important attributes of welds, fusion zone geometry, cooling rates and solidification parameters were studied during double pulsed gas metal arc welding of an aluminum alloy. A comprehensive, three-dimensional numerical heat transfer and fluid flow model was developed and tested with experimental data. Effects of current amplitude on fusion zone geometry, solidification parameters, and weld microstructures of DP-GMAW were studied. Below are the specific findings.

- (1) For a given heat input, the average cooling rates during double pulsed gas metal arc welding could be altered by changing pulsing parameters. In contrast with single pulsed welding, double pulsed welding resulted in considerable temporal variation of fusion zone geometry, local cooling rates and solidification parameters. Remelting and resolidification of the previously solidified metal near the trailing edge of the weld pool significantly affected the thermal cycles, solidification parameters and the microstructure of the fusion zone of an aluminum alloy.
- (2) Adjustment of the current amplitude while keeping the heat input constant resulted in significant changes in the fusion zone attributes. Apart from the anticipated temporal changes in the fusion zone geometry, the average cooling rate was significantly affected by the current amplitude at a constant heat input. Thus, the average cooling rate could be adjusted by changing current amplitude instead of heat input.
- (3) Solidification growth rate and cooling rate during double pulsed gas metal arc welding were found to be significantly higher than those of the single pulsed variety. Microstructural characterization of an aluminum alloy fusion zone showed finer grains consistent with faster cooling rate during double pulsed gas metal arc welding.

Conflicts of interest

The authors declare that there is no conflict of interest regarding the publication of this paper.

Acknowledgements

One of the authors acknowledges financial support for this research from the High Leading Talent Introduction Program of GDAS (2016GDASRC-0106); Industry-university-research Program of Guangdong Province and the Ministry of Education (2013B090600098); and the SCUT Doctoral Student Short-Term Overseas Visiting Study Funding Project.

References

- David, S.A., DebRoy, T., 1992. Current issues and problems in welding science. *Science* 257, 497–502. <http://dx.doi.org/10.1126/science.257.5069.497>.
- David, S.A., Vitek, J.M., 1989. Correlation between solidification parameters and weld microstructures. *Int. Mater. Rev.* 34, 213–245. <http://dx.doi.org/10.1179/imr.1989.34.1.213>.
- Kim, C.H., Zhang, W., DebRoy, T., 2003. Modeling of temperature field and solidified surface profile during gas-metal arc fillet welding. *J. Appl. Phys.* 94, 2667–2679. <http://dx.doi.org/10.1063/1.1592012>.
- Liu, A., Tang, X., Lu, F., 2013a. Arc profile characteristics of Al alloy in double-pulsed GMAW. *Int. J. Adv. Manuf. Technol.* 65, 1–7. <http://dx.doi.org/10.1007/s00170-012-4141-0>.
- Liu, A., Tang, X., Lu, F., 2013b. Study on welding process and prosperities of AA5754 Al-alloy welded by double pulsed gas metal arc welding. *Mater. Des.* 50, 149–155. <http://dx.doi.org/10.1016/j.matdes.2013.02.087>.
- Liu, C.Y., Wang, Q., Jia, Y.Z., Zhang, B., Jing, R., Ma, M.Z., Jing, Q., Liu, R.P., 2013c. Evaluation of mechanical properties of 1060-Al reinforced with WC particles via warm accumulative roll bonding process. *Mater. Des.* 43, 367–372. <http://dx.doi.org/10.1016/j.matdes.2012.07.019>.
- Liu, J.W., Rao, Z.H., Liao, S.M., Tsai, H.L., 2015. Numerical investigation of weld pool behaviors and ripple formation for a moving GTA welding under pulsed currents. *Int. J. Heat Mass Transf.* 91, 990–1000. <http://dx.doi.org/10.1016/j.ijheatmasstransfer.2015.08.046>.
- Mathivanan, A., Devakumaran, K., Kumar, A.S., 2014. Comparative study on mechanical and metallurgical properties of AA6061 aluminum alloy sheet weld by pulsed current and dual pulse gas metal arc welding processes. *Mater. Manuf. Process.* 29, 941–947. <http://dx.doi.org/10.1080/10426914.2014.912314>.
- Mishra, S., Lienert, T.J., Johnson, M.Q., DebRoy, T., 2008. An experimental and theoretical study of gas tungsten arc welding of stainless steel plates with different sulfur concentrations. *Acta Mater.* 56, 2133–2146. <http://dx.doi.org/10.1016/j.actamat.2008.01.028>.
- Roy, G.G., Elmer, J.W., DebRoy, T., 2006. Mathematical modeling of heat transfer, fluid flow, and solidification during linear welding with a pulsed laser beam. *J. Appl. Phys.* 100, 034903. <http://dx.doi.org/10.1063/1.2214392>.
- Sen, M., Mukherjee, M., Pal, T.K., 2015. Evaluation of correlations between DP-GMAW process parameters and bead geometry. *Weld. J.* 94, 265S–279S.
- Wang, L.L., Lu, F.G., Cui, H.C., Tang, X.H., 2014. Investigation of molten pool oscillation during GMAW-P process based on a 3D model. *J. Phys. D: Appl. Phys.* 47, 465204. <http://dx.doi.org/10.1088/0022-3727/47/46/465204>.
- Wang, L.L., Heng, G.C., Chen, H., Xue, J.X., Lin, F.L., Huang, W.J., 2016a. Methods and results regarding sinusoid modulated pulse gas metal arc welding. *Int. J. Adv. Manuf. Technol.* 86, 1841–1851. <http://dx.doi.org/10.1007/s00170-015-8267-8>.
- Wang, L.L., Jin, L., Huang, W.J., Xu, M., Xue, J.X., 2016b. Effect of thermal frequency on AA6061 aluminum alloy double pulsed gas metal arc welding. *Mater. Manuf. Process.* 31, 2152–2157. <http://dx.doi.org/10.1080/10426914.2015.1103863>.
- Wang, L.L., Wei, H.L., Xue, J.X., DebRoy, T., 2017a. A pathway to microstructural refinement through double pulsed gas metal arc welding. *Scr. Mater.* 134, 61–65. <http://dx.doi.org/10.1016/j.scriptamat.2017.02.034>.
- Wang, Y., Qi, B., Cong, B., Yang, M., Liu, F., 2017b. Arc characteristics in double-pulsed VP-GTAW for aluminum alloy. *J. Mater. Process. Technol.* 249, 89–95. <http://dx.doi.org/10.1016/j.jmatprotec.2017.05.027>.
- Wei, H.L., Pal, S., Manvatkar, V., Lienert, T.J., DebRoy, T., 2015. Asymmetry in steel welds with dissimilar amounts of sulfur. *Scr. Mater.* 108, 88–91. <http://dx.doi.org/10.1016/j.scriptamat.2015.06.024>.
- Wei, H.L., Elmer, J.W., DebRoy, T., 2016. Origin of grain orientation during solidification of an aluminum alloy. *Acta Mater.* 115, 123–131. <http://dx.doi.org/10.1016/j.actamat.2016.05.057>.
- Wei, H.L., Elmer, J.W., DebRoy, T., 2017. Three-dimensional modeling of grain structure evolution during welding of an aluminum alloy. *Acta Mater.* 126, 413–425. <http://dx.doi.org/10.1016/j.actamat.2016.12.073>.
- Yamamoto, H., Harada, S., Ueyama, T., Ogawa, S., 1992. Development of low-frequency pulsed MIG welding for aluminium alloys. *Weld. Int.* 6, 580–583. <http://dx.doi.org/10.1080/09507119209548246>.
- Yamamoto, H., Harada, S., Ueyama, T., Ogawa, S., Matsuda, F., Nakata, K., 1993. Beneficial effects of low-frequency pulsed MIG welding on grain refinement of weld metal and improvement of solidification crack susceptibility of aluminium alloys: study of low-frequency pulsed MIG welding. *Weld. Int.* 7, 456–461. <http://dx.doi.org/10.1080/09507119309548425>.